

Transmon platform for quantum computing challenged by chaotic fluctuations

Christoph Berke,¹ Evangelos Varvelis,^{2,3} Simon Trebst,¹ Alexander Altland,¹ and David P. DiVincenzo^{2,3,4}

¹*Institute for Theoretical Physics, University of Cologne, 50937 Cologne, Germany*

²*Institute for Quantum Information, RWTH Aachen University, 52056 Aachen, Germany*

³*Jülich-Aachen Research Alliance (JARA), Fundamentals of Future Information Technologies, 52425 Jülich, Germany*

⁴*Peter Grünberg Institute, Theoretical Nanoelectronics, Forschungszentrum Jülich, 52425 Jülich, Germany*

(Dated: March 15, 2022)

From the perspective of many body physics, the transmon qubit architectures currently developed for quantum computing are systems of coupled nonlinear quantum resonators. A significant amount of intentional frequency detuning (‘disorder’) is required to protect individual qubit states against the destabilizing effects of nonlinear resonator coupling. Here we investigate the stability of this variant of a many-body localized (MBL) phase for system parameters relevant to current quantum processors of two different types, those using untunable qubits (IBM type) and those using tunable qubits (Delft/Google type). Applying three independent diagnostics of localization theory — a Kullback-Leibler analysis of spectral statistics, statistics of many-body wave functions (inverse participation ratios), and a Walsh transform of the many-body spectrum — we find that these computing platforms are dangerously close to a phase of uncontrollable chaotic fluctuations.

I. INTRODUCTION

When subject to strong external disorder, wave functions of many body quantum systems may show *many-body localization* (MBL) in states defined by (but not in trivial ways) the eigenstates of the disordering operators. A standard paradigm in this context is the spin- $\frac{1}{2}$ Heisenberg chain in a random z -axis magnetic field. Here, the disorder basis comprises the ‘physical’ p -qubits [1] defined by the spin states, different due to spin exchange from the eigenbasis of ‘localized’ l -qubits [2, 3]. The latter are stationary but remain non-trivially correlated, including in the deeply localized phase.

Although it may seem paradoxical at first sight, strong intentional ‘disordering’ and MBL in the above sense are a vitally important resource in the most advanced quantum computing (QC) platform available to date, the superconducting transmon qubit array processor. Physically, the transmon array is a system of coupled nonlinear quantum oscillators. At the low energies relevant to QC the system becomes equivalent to the negative U Bose Hubbard model. Site occupations 0 and 1 define the transmon p -qubit states, known as ‘bare qubits’ in QC language. Massive deliberate randomization of the individual qubit energies maintains the integrity of these states in the presence of the finite inter-transmon coupling required for computing functionality. This coupling makes the eigen- l -qubits of the system different from the p -qubits. Considerable efforts are invested in the characterization and control of the induced correlations, known as ZZ couplings in the parlance of the QC community [4].

Connections between MBL and superconducting qubits have been considered earlier [5, 6], but mainly with a focus on applications of qubit arrays as quantum simulators of the bosonic MBL transition [6]. Surprisingly, however, the obvious reverse question has not been asked systematically so far: what bearings may qubit isolation by disorder have on QC functionality? Reliance on strong disorder localization is a Faustian approach inasmuch as it accepts the presence of *quantum chaos*, which is an arch-enemy of quantum device control of any kind. Lowering the strength of disorder

brings one closer to the MBL-to-chaos transition, heralded by a growth of l -qubit correlations as early indicators for the proximity of the uncontrollable chaotic phase. Since the key requirement of QC, the execution of gate operations, requires on-demand rapid growth of entanglement between l -qubits, it is imperative that some definite amount of coupling is present. A crucial question that we confront, therefore, is whether this necessary level of coupling will still keep us outside the chaotic zone.

In this paper [7], we address this question by application of state-of-the-art diagnostic tools of MBL theory to realistic models of qubit arrays employed in the experimental efforts by the groups of Delft [8], Google [9], IBM [10], and others. We monitor departures from the limit of strong localization in the spectral and spatial correlations of many- l -qubit wave functions, and analyze the growth of l -qubit correlations. Considering small instances of multi-transmon systems we find that the phase boundary between MBL and quantum chaos indeed lies dangerously close to the parameter ranges of current experiments. We also find that increasing the coordination number of the transmon lattice, as necessary for 2D connected transmon networks, decidedly increases many-body delocalization and the incipient chaos of the dynamics. Our work warns that further progress towards larger QCs will be dependent on skirting the dangerous attributes of chaotic parts of the parameter space.

II. TRANSMON ARRAY HAMILTONIAN

Our study begins with the well-established minimal model for interacting transmon qubits [11]:

$$H = 4E_C \sum_i n_i^2 - \sum_i E_{J_i} \cos \phi_i + T \sum_{\langle i,j \rangle} n_i n_j. \quad (1)$$

Here, n_i is the Cooper-pair number operator of transmon i , conjugate to its superconducting phase ϕ_i . The transmon charging energy, E_C , is determined by the capacitance of the metal body of the transmon, and is easily fixed at a desired

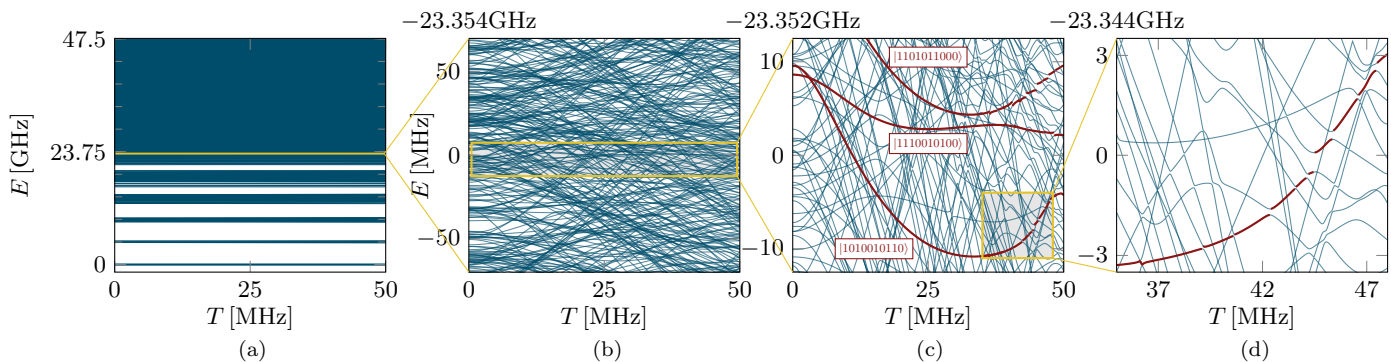


FIG. 1. **Energy spectrum of a coupled transmon array.** Illustrated are the energy levels $E_\alpha(T)$ of Hamiltonian Eq. (1) on varying energy scales; data shown is for a coupled transmon chain of length $N = 10$. Panel (a) illustrates the clustering of levels into energy bundles corresponding to the total number of bosonic excitations. Panel (b) zooms into the 5-excitation band, which upon further enlargement in panel (c) reveals level repulsions that become particularly visible for larger couplings. In panel (c) we also mark in red a number of computational states (identified in this energy window at vanishing coupling $T = 0$). The further zoom-in of panel (d) traces one such computational state through a sequence of avoided crossings.

constant, typically about $E_C = 250$ MHz ($\hbar = 1$). The Josephson-junction charging energy, E_J , is proportional to the critical current of the junction. It is difficult to fix this constant reproducibly to better than a few percent. However, typical values lie in the vicinity of around 12.5 GHz, much larger than the charging energy. Finally, electrical coupling between the transmons, often via a capacitance, produces the charge coupling Tn_in_j . The coefficient T has varied over a substantial range in 15 years of experiments [12]; T values beyond 50 MHz are possible, but current experiments are primarily in the range $T = 5 - 20$ MHz, making T the smallest energy scale in the problem.

The descent from the above minimal model to an effective low energy limit of coupled qubits proceeds via a realization of an attractive Bose-Hubbard model as an intermediate stage. Applying a sequence of approximations to Eq. (1) (series expansion of the Josephson characteristic, rotating wave approximation) one arrives at the model

$$\begin{aligned}
 H = & \sum_i \nu_i a_i^\dagger a_i - \frac{E_C}{2} \sum_i a_i^\dagger a_i (a_i^\dagger a_i + 1) \\
 & + \sum_{\langle i,j \rangle} t_{ij} (a_i a_j^\dagger + a_i^\dagger a_j), \\
 \nu_i \equiv & \sqrt{8E_{J_i} E_C}, \quad t_{ij} = \frac{T}{4\sqrt{2}E_C} \sqrt{E_{J_i} E_{J_j}}. \quad (2)
 \end{aligned}$$

To leading order, this model describes the transmon as a harmonic oscillator, where the above choices of energy scales place the frequencies $\nu_i \approx 6$ GHz in the middle of a microwave frequency band convenient for precision control. The disorder necessary for localization, and thus the proper functioning of the transmon array as a qubit register, is produced by variations of E_J . The attraction term, a remnant of the cos-nonlinearity, is considerably smaller than the average harmonic term, which is desired for transmon operation. Finally, the characteristic strength of the nearest neighbor hopping coefficients, $|t_{ij}| \approx \frac{T}{4\sqrt{2}} \sqrt{\frac{E_J}{E_C}} \equiv J$, continues to be the smallest

energy scale in the problem.

Eq. (2) is a reference model for bosonic MBL. As mentioned above, inevitable variations of E_J are in the percent range; thus, at a minimum, there is variation of ν_i of around $\delta\nu_i \approx 60$ MHz. This scale is much larger than the particle hopping strength, which for the same parameter set is about $J \approx 6$ MHz. At these values, we can hope that the system is in the MBL phase, and we confirm this below.

The above ‘natural disorder’ regime has been in use in the many generations of quantum computer processors [10] that IBM has provided on its cloud service since 2016. Other quantum computing research has often chosen to build in additional disorder intentionally, but without awareness of its relevance for MBL physics. This research is exemplified, for example, in the recent reports from TU Delft on their extensible module for surface-code implementation [8], and by Google of its 53-qubit processor [9]. So below, we will consider IBM vs. Delft/Google parameter ranges for assessing the incipient quantum chaos that is, in fact, present in both settings. For all the model calculations we present, we represent this disorder by drawing independent samples from a Gaussian distribution with standard deviation δE_J , added to the mean Josephson energy E_J . For the IBM case δE_J is around 500 MHz (for a typical E_J of 12.5 GHz), while for the Delft/Google case δE_J is some 10 times larger (precise numbers are given below).

For the IBM parameters, the energy eigenvalues of Eq. (1) cluster into energy bundles corresponding to the total number of bosonic excitations, as shown in Fig. 1(a). Looking inside the 5-excitation band, we see (in Fig. 1(b)) a dense tangle of energy levels. Only some of these levels are used to perform quantum computation in IBM quantum processors; the identification of these levels, as shown in Fig. 1(c) and discussed in detail in Sec. III C, can only be done unambiguously if we are far away from the chaotic phase.

Having QC applications in mind, we are primarily interested in signatures of quantum chaos in the ‘computational subspace’ of the bosonic Hilbert space, i.e. the space com-

prising local occupation numbers $a_i^\dagger a_i = 0, 1$ as p -qubit states for QC. In that Hilbert space sector, the problem reduces to a disordered spin- $1/2$ chain, another paradigm of MBL. Recent results from the MBL community indicate that the separation into a chaotic ergodic and an integrable localized phase is not as straightforward as previously thought, and that wave functions show remnants of extendedness and fractality even in the ‘localized’ phase [13].

III. DIAGNOSTICS

In the following, we analyze the Hamiltonian Eq. (1) by a combination of different numerical methods tailored to the description of localized phases:

- *Spectral statistics*: According to standard wisdom, many-body spectra have Wigner-Dyson statistics in the phase of strongly correlated chaotic states, and Poisson statistics in that of uncorrelated localized states. Real systems show more varied behavior, quantified below in terms of the Kullback-Leibler divergence. This produces a charting of parameter space indicating the chaos/MBL boundary and the rapidity at which the boundary is approached.
- *Wave function statistics*: Focusing on the localization regime, we analyze how strongly the eigenstates differ from the localized states of the strictly decoupled system.
- *Walsh transform*: We will quantify the correlations between l -qubits (known in the QC community as ZZ couplings, and in the MBL community as τ -Hamiltonian tensor coefficients) by application of a Walsh transform filter. To the best of our knowledge, this particularly sensitive tool has not been applied so far to the diagnostics of MBL.

As a principal example we consider a system of N coupled transmons in a one-dimensional chain geometry – a minimalistic setting that allows us to probe essential aspects of localization physics and quantum chaos using the above diagnostics and whose computational feasibility allows us to map out the broader vicinity of experimentally relevant parameter regimes. Typical system sizes vary between $N = 5 \dots 10$ sites, as detailed below.

A. Spectral statistics

We probe the spectral signatures of this coupled transmon system in an energy bundle of excited states (see Fig. 1(b)), which are generated by a total of $N/2 = 5$ bit flips and can be viewed as typical representatives in the computational subspace [14]. Zooming in on this mid-energy spectrum, we analyze the distribution of the ratios of adjacent level spacings $r_n = \Delta E_n / \Delta E_{n+1}$ [15] (in order to avoid level unfolding) by comparing to what is expected for these ratios in Poisson

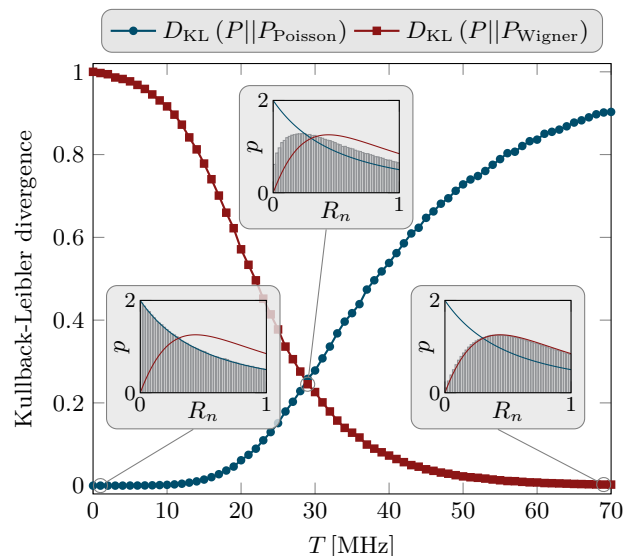


FIG. 2. **Spectral statistics** of a chain of $N = 10$ transmons versus the coupling parameter T for fixed average Josephson energy $E_J = 44$ GHz with small site-to-site variations characteristic of the IBM design. These statistics indicate a transition from Poisson statistics (blue) in the MBL regime (at low coupling) to Wigner-Dyson statistics (red) in a many-body delocalized regime (at large coupling). Shown are normalized Kullback-Leibler (KL) divergences calculated for the distribution of ratios of consecutive level spacings in the energy spectrum, such as the ones illustrated in the insets for three characteristic couplings. Note that we plot $R_n = \min(r_n, 1/r_n)$ in order to restrict to the range $[0, 1]$. The KL divergences are normalized such that $D_{\text{KL}}(P_{\text{Wigner}}||P_{\text{Poisson}}) = 1$ and vice versa.

or Wigner-Dyson statistics. This is often done via qualitative observations, such as focusing on the limit of $r \rightarrow 0$, where the distribution exhibits a maximum for Poisson statistics, but completely vanishes for Wigner-Dyson statistics (see, e.g., the insets of Fig. 2). However, a recent study [16] (of a Fock space localization transition) has shown that such inspections may trick one into false conclusions and that the Kullback-Leibler (KL) divergence [17] provides a far more reliable quantitative alternative. The KL divergence

$$D_{\text{KL}}(P||Q) = \sum_k p_k \log \left(\frac{p_k}{q_k} \right), \quad (3)$$

defines an entropic measure quantifying the logarithmic difference between two distributions P and Q . In our case, the p_k are extracted from the numerical spectrum for a given set of parameters, while the q_k follow one of the two principal spectral statistics considered here.

As shown in the main panel of Fig. 2, this KL divergence vanishes when calculated with regard to the Poisson distribution for small transmon couplings, indicating perfect agreement with the expectation for an MBL phase (also corroborated by the striking visual match of the distributions in the corresponding inset of Fig. 2), while it is maximal when compared to Wigner-Dyson statistics (red curve in Fig. 2). This picture is inverted for larger transmon couplings $T \approx$

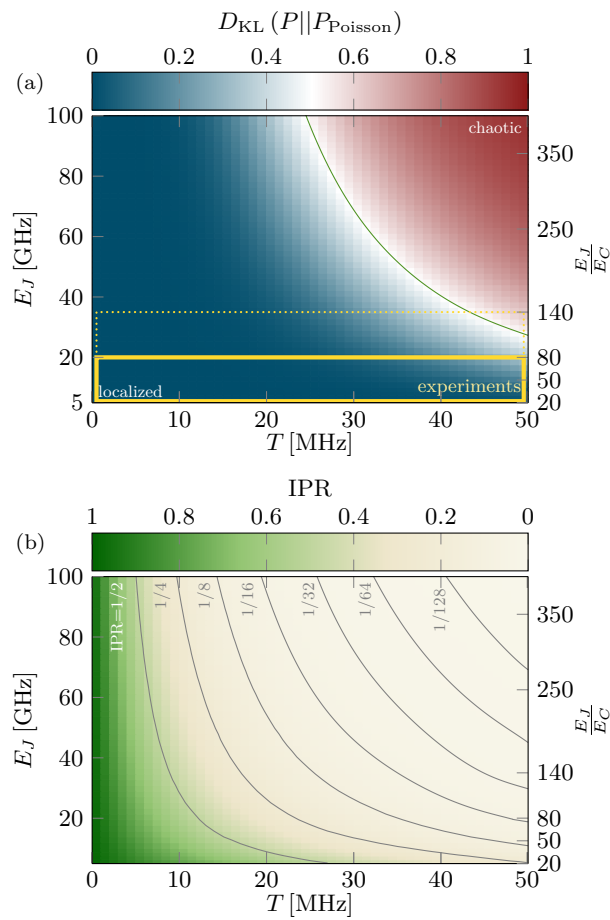


FIG. 3. **Phase diagrams** in the plane spanned by the Josephson energy E_J and the transmon coupling T . The upper panel summarizes the *spectral statistics* by plotting the Kullback-Leibler divergence with regard to the Poisson distribution, identifying an MBL regime (blue) for small couplings and a quantum chaotic regime (red) following Wigner-Dyson statistics for large couplings. The lower panel summarizes the *wave function statistics* by color-coding the inverse participation ratio (IPR) showing a fast drop to values below $1/2$ already for moderate coupling strength. The grey lines indicate contour lines of constant IPR.

70 MHz, where we find an extremely good match to Wigner-Dyson statistics – unambiguous evidence for the emergence of strongly correlated chaotic states. Probably even more important is the fact that these KL divergences allow us to quantify proximity to the diametrically opposite regimes for all intermediate coupling parameters. This includes a region of ‘hybrid statistics’ around the crossing point of the two curves, indicating an equal distance from both limiting cases, which we will discuss in more detail below.

By way of this KL divergence one can then map out an entire phase diagram, e.g. in the plane spanned by varying values of the transmon coupling and Josephson energy, while fixing the charging energy as shown in Fig. 3 (for IBM parameters). This allows us to clearly distinguish the existence of two regimes, the expected MBL phase (colored in blue) for

small transmon coupling and a quantum-chaotic regime (colored in red), where the level statistics follows Wigner-Dyson behavior (with delocalized, but strongly correlated states) for sufficiently strong transmon couplings. It is this latter regime that one surely wants to avoid in any experimental QC setting – but before we discuss the experimental relevance of our results, we want to characterize more deeply the quantum states away from this chaotic regime using another diagnostic.

B. Wave function statistics

One particularly potent measure of the degree to which a given wave function is localized or delocalized, is its inverse participation ratio (IPR)

$$\text{IPR} = \int dr |\psi(r)|^4, \quad (4)$$

i.e. its second moment. An IPR of 1 indicates a completely localized state (as in our example for vanishing coupling $T = 0$), while an IPR less than 1 indicates the tendency of a wave function towards delocalization [18].

Here we consider the IPR measured as an average over all states in one of the energy bundles illustrated in Fig. 1(a), e.g. the manifold of typical states with $N/2 = 5$ bit flips considered in the spectral statistics above. The lower panel of Fig. 3 shows the IPR in the same parameter space as its top panel. What is most striking here is that the IPR rapidly decays – the contour lines in the panel indicate exponentially decaying levels of $1/2, 1/4, 1/8, \dots, 1/128$ – indicating that the wave functions quickly delocalize. Note in particular, that the IPR has dropped to a value of less than 10% in the region of ‘hybrid statistics’ identified in the level spectroscopy above.

A particularly consistent picture emerges if one performs a simple rescaling of the numerical data in both panels of Fig. 3. As shown in Fig. 4 below, the individual traces of both the KL divergence and the IPR for varying values of the Josephson energy E_J (shown in the insets) all collapse onto one another when rescaling the coupling parameter $T \rightarrow TE_J^\mu$ with the exponent μ being the single free parameter. Such a data collapse is typically considered strong evidence for the existence of a *phase transition*, i.e. we can manifestly separate the MBL phase for small transmon couplings from a truly chaotic phase for sufficiently large couplings. This also allows us to mark a Rubiconian line into our phase diagram (indicated by the green line in the top panel) that should not be crossed in any quantum computation scheme, as all exquisitely prepared quantum information would be instantly lost upon entering the realm of quantum chaos lying beyond. The data collapse at a value $\mu \simeq 0.5$ follows from a simple argument: thinking of the wave functions as states defined on a high dimensional lattice defined by the occupation number configurations $n = (n_1, n_2, \dots, n_N)$ ($n_i = 0, 1$ for the computational subspace), individual sites, n are connected to a large number Z of neighbors via the ‘hopping matrix elements’, t_{ij} . Wave functions hybridize over these two sites, provided $|t_{ij}| \gtrsim |\Delta\epsilon_{nm}|$, where $\Delta\epsilon_{nm}$ is of the energy difference between the two sites in the limit $t \rightarrow 0$. Inspection of Eq. (2)

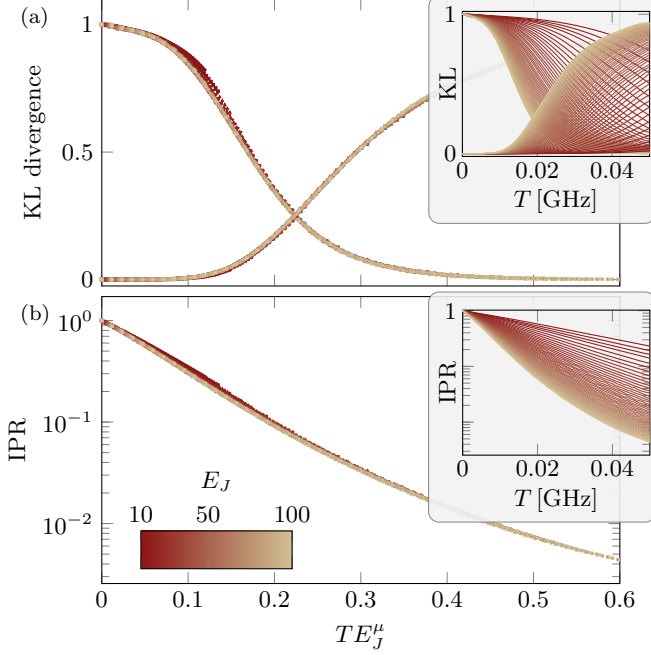


FIG. 4. **Data collapse** of the individual traces of the KL divergence and IPR, underlying the phase diagrams of Fig. 3 and shown in the two insets, by rescaling the coupling parameter with regard to the Josephson energy as $T \rightarrow TE_J^\mu$ with an exponent $\mu \approx 0.54$.

shows that $\Delta\epsilon_{nm} \sim E_{J_i}^{1/2} - E_{J_j}^{1/2} \sim E_J^{-1/2}(E_{J_i} - E_{J_j})$. In our analysis, the random deviations are scaled such that $(E_{J_i} - E_{J_j}) \sim E_J^{1/2}$, such that $\Delta\epsilon_{nm}$ is effectively independent of E_J . However, $t_{ij} \sim TE_J^{1/2}$, indicating that $TE_J^{1/2}$ is the relevant scaling variable for the transition where the two parameters T and E_J are concerned.

C. Walsh-transform analysis

The MBL phase is the right place to be for quantum computing, since computational qubits (the l -qubits above) retain their identity there. But, as indicated by the drop of IPR, even the localized phase may be problematic. Here we apply another diagnostic that is specifically adapted to identifying problems with running a quantum computation in the MBL phase. It begins with the expectation, announced in [2, 3], that the Hamiltonian of the multi-qubit system, in the l -qubit basis, can be expressed as

$$\begin{aligned}
 H &= \sum_i h_i \tau_i^z + \sum_{ij} J_{ij} \tau_i^z \tau_j^z + \sum_{i,j,k} K_{ijk} \tau_i^z \tau_j^z \tau_k^z + \dots (5) \\
 &= \sum_{\mathbf{b}} c_{\mathbf{b}} Z_1^{b_1} Z_2^{b_2} \dots Z_N^{b_N}. (6)
 \end{aligned}$$

Eq. (5), the ' τ -Hamiltonian' of MBL theory [2, 3], embodies the observation that a diagonalized Hamiltonian can be written in a basis of diagonal operators, here τ_i^z , that is to

say Pauli-Z operators (Z_i) in the quantum-information terminology of Eq. (6). Here the sum is over N -bit strings $\mathbf{b} = b_1 b_2 \dots b_N$, where each b_i is 0 or 1.

A system described by the τ -Hamiltonian can be an excellent data carrier for a quantum computer, particularly if the high-weight terms are small. If only the one-body terms in Eq. (5) are non-zero, the system is an ideal quantum memory: In the interaction frame, defined by the non-entangling unitary transformation $U(t) = \exp(it \sum_i h_i \tau_i^z)$, all quantum states, including entangled ones, remain stationary. Unfortunately, the expectation of MBL theory is that the two-body and higher interaction terms are non-zero and grow as the chaotic phase is approached.

We have performed a numerical extraction of the parameters of Eqs. (5-6) for a 5-transmon chain. We find that problematic departures from full localization do indeed occur already at rather small values of the qubit-qubit coupling parameter T . This reinforces the message, in a *basis-independent* way, of our IPR study. But this extraction must begin with a very non-trivial step, namely the identification of the qubit eigenenergies of the transmon Hamiltonian. Since this Hamiltonian Eq. (1) is bosonic, it has a much larger Hilbert space than the spin- $1/2$ view embodied in Eqs. (5-6). The qubit states, those with bosonic occupations limited to 0 and 1, are not separated in energy from the others, but are fully intermingled with states of higher occupancy, as illustrated in Fig. 1(c). It would thus appear that this truncation is rather unnatural; but it is in fact crucial to the whole quantum computing program with transmons. It is essential to pick out, from all the eigenlevels E_α of the full Hamiltonian Eq. (1) as shown in Fig. 1, just the subset of levels $E_{\mathbf{b}}$ that can be associated with a bitstring label \mathbf{b} (cf. Eq. (6)).

We find that there is a workable procedure for this truncation, which however starts to become problematic long before we reach the MBL-chaotic phase boundary. We adopt the following assignment procedure: at $T = 0$ all states have exact bosonic quantum numbers, so the 2^N eigenstates with bitstring label \mathbf{b} (the Walsh transforms of the bitstrings in Eq. (6), as explained shortly) are immediately identified there. We increase T ; as long as no near-crossings of energy levels occur, the labeling remains unchanged. We then find that the first near-crossings that occur have the character of isolated anti-crossings with very small gaps. In this situation we can confidently associate the label \mathbf{b} with the diabatic state (i.e., the

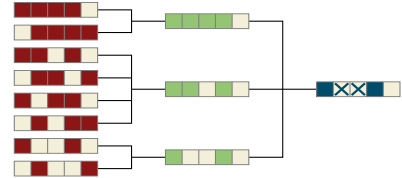


FIG. 5. **Color-coding of Walsh coefficients** for a system of five transmon qubits. The first column shows the individual qubit assignments (light color = '0', red color = '1'), the second and third columns indicate ways to average coefficients according to the enclosing brackets.

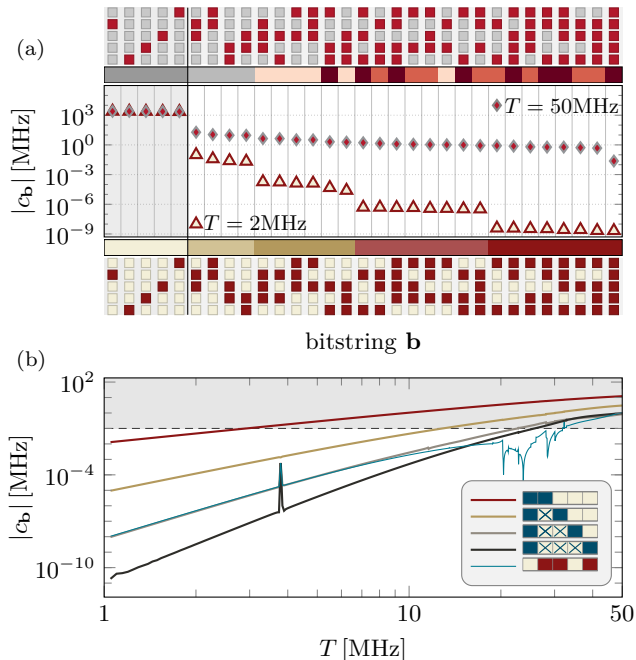


FIG. 6. **Walsh-transform analysis.** (a) Comparison of the different coefficients for two values of the coupling T , for the IBM parameters. The narrow colored bars between the bitstring / x -axis and the plot shows the maximal distance between two 1's in the bitstrings. (b) Absolute value of averaged Walsh coefficients as a function of the coupling T , where the averaging is done over coefficients with bitstring labels of equal maximal distance of two 1's. Also shown is the absolute value of the Walsh coefficient with bitstring label 01101 for comparison. For the legend see also Fig. 5.

one that goes straight through the anticrossing). We show this by the coloring of Fig. 1(c). Empirically, this identification procedure works through many anticrossings, up to about half way to the phase transition; gradually, gaps become larger, and identification of qubit states becomes more ambiguous (Fig. 1(d)). Naturally, in the chaotic phase, eigenstate thermalization says that there is no hope of consistently identifying any eigenstates as information-carrying multi-qubit states.

Having performed this state identification and tagged the subset of eigenlevels $E_{\mathbf{b}}(T)$ that can be identified as qubit states, the coefficients of the τ -Hamiltonian are easily obtained by a Walsh-Hadamard transform [19]:

$$\begin{aligned} c_{\mathbf{b}}(T) &= \frac{1}{2^N} \sum_{\mathbf{b}'} (-1)^{b_1 b'_1} (-1)^{b_2 b'_2} \dots (-1)^{b_N b'_N} E_{\mathbf{b}'}(T) \\ &= \frac{1}{2^N} \sum_{\mathbf{b}'} (-1)^{\mathbf{b} \cdot \mathbf{b}'} E_{\mathbf{b}'}(T). \end{aligned} \quad (7)$$

Being a kind of Fourier transform, the Walsh transform functions to extract correlations, in this case in the correlations of the computational eigenstates (in energy). Fig. 6 shows these coefficients vs. T . For small T , many of the expectations from MBL theory [2, 3] are fulfilled: There is a clear hierarchy according to the locality of the coefficients. Thus,

nearest-neighbor ZZ interactions are the largest, followed by second-neighbor ZZ and contiguous ZZZ couplings, and so forth. Jumps occur in these coefficients, initially very small, which arise from the switching of labeling at anticrossings.

IV. INCIPIENT CHAOS IN CURRENT SUPERCONDUCTING QUANTUM COMPUTERS

Superconducting quantum computers have scored impressive achievements in recent years, all the more remarkable given the potential we see for grave difficulties in this physical platform. The Hamiltonian of this platform unquestionably has a quantum-chaotic regime, in which useful, controllable computing is simply impossible. Not surprisingly, successful devices have, according to our analysis, managed to avoid this regime. As we have argued above, the many-body localized phase is surely the place where the conditions for quantum computing become possible. But even the MBL phenomenology presents obstacles, and we will consider here how serious these might be.

A. IBM parameters

We first focus on the IBM parameters above. IBM successfully made cloud quantum computing available with a 5-transmon device in 2016, and has had many satisfied users. While ‘stress tests’ of their devices have sometimes revealed problems [20], successive generations of chips have seen steady improvement in performance, as indicated by IBM’s ‘quantum volume’ metric [21].

Our diagnostics indicate that this success has been possible by treading a narrow path, with danger from several directions. Because of the details of the chosen two-qubit entangling gate using the ‘cross-resonance’ technique [22], IBM must maintain small disorder, $\delta\nu < E_C$, which results in a transition to chaos occurring around $T = 70$ MHz when $E_J = 20$ GHz. While such parameters are perfectly possible in transmon arrays, IBM has prudently worked at T values far below this. The transmon coupling T , however, cannot be made arbitrarily low, because the speed of execution of quantum gates is proportional to T . Thus, in order to compete successfully with relaxation effects, T values of at least 1 MHz would certainly be necessary.

All IBM-style devices have operated in the range $T = 5 - 20$ MHz, which would seem to fit comfortably between the limits of relaxation effects on the one hand and quantum chaos on the other. While indeed this looks like a rather safe zone from the point of view of our Kullback-Leibler diagnostic Fig. 3(a), we see that this is already a regime where IPR values fall well below 1 (Fig. 3(b)). Thus, qubits in these devices should be significantly dressed. This certainly complicates the point of view of the data carriers in these computers, in that a physical transmon no longer is the exclusive container of the localized qubit. Such dressing is not necessarily an impediment to quantum computing, and various

authors have shown that consistent quantum computing with perturbatively dressed states is indeed possible [23–25].

Our Walsh diagnostic indicates perhaps the most serious impediments that IBM scientists face in achieving reliable quantum computing with their devices. The ‘ τ -Hamiltonian’ phenomenology of MBL theory, analyzed for the parameter range of interest in Fig. 6, indicates the potential problems that are faced in quantum-computer operation. The problems begin with the weight-two terms (J_{ij}) of Eq. (5) (as mentioned above, weight-one terms present no difficulty). These two-body (ZZ) terms are indeed known and carefully analysed in transmon research [4, 26, 27]. Their troublesome consequences, including dephasing of general qubit states, and failure to commute with quantum gate operations, have been ameliorated by refocusing strategies which, while effective, add costly overhead to quantum computer operations. The mathematical basis of these strategies were established in the Hadamard-matrix techniques of Ref. 28, which show that the strategies are formally efficient. Practically speaking, however, added overhead at some point becomes insupportable in the face of relaxation penalties and a practical value of $J_{ij} \sim 50 - 100$ kHz has been recognized as an upper limit of ZZ couplings that can be tolerated.

This limit has been marked (dashed line) in Fig. 6(b). We see that it is exceeded already at $T = 3$ MHz. This is only for one particular disorder realization with $\delta E_J = 0.675$ GHz, and we note that there is significant variation of this crossover point for different realizations from the ensemble of 5-transmon chains. IBM has certainly selected the best chips for its cloud offering, and has been able to field devices with somewhat larger T . But we see that all coefficients of the τ -Hamiltonian grow rapidly with T . We observe a clear hierarchy of magnitudes of the coefficients in Eqs. (5-6), i.e. a power-law growth with powers increasing with the order and degree of locality of the terms. Even the simplest higher order terms, that is ZZZ terms, have never been considered in transmon research. No generalization of the Hadamard-matrix theory of Ref. 28 has been worked out. By the time T reaches 10 – 20 MHz, ZZZ terms and a multitude of other contributions of all weights become roughly comparable, and noticeable jumps (clearly seen in Fig. 6(b)) reflect the growing ambiguity of identifying multi-qubit states. We would judge that in this regime quantum computing is well-nigh impossible, even though the phase transition is still a long way off.

B. Delft/Google parameters

Other techniques for executing entangling gates leave considerably more freedom to increase the disorder, with $\delta\nu$ values in the GHz range. This option can forestall the growth of problematic precursors of chaotic behavior. A good example of a quantum computer that uses this freedom is the surface-7 device of TU Delft [8]. During gate operation the qubit frequencies are temporarily tuned into resonant conditions that ‘turn on’ entanglement generation. This is done in a pattern that does not lead to any extensive delocalization. In the notable 53-qubit quantum computer of Google [9], this tuning

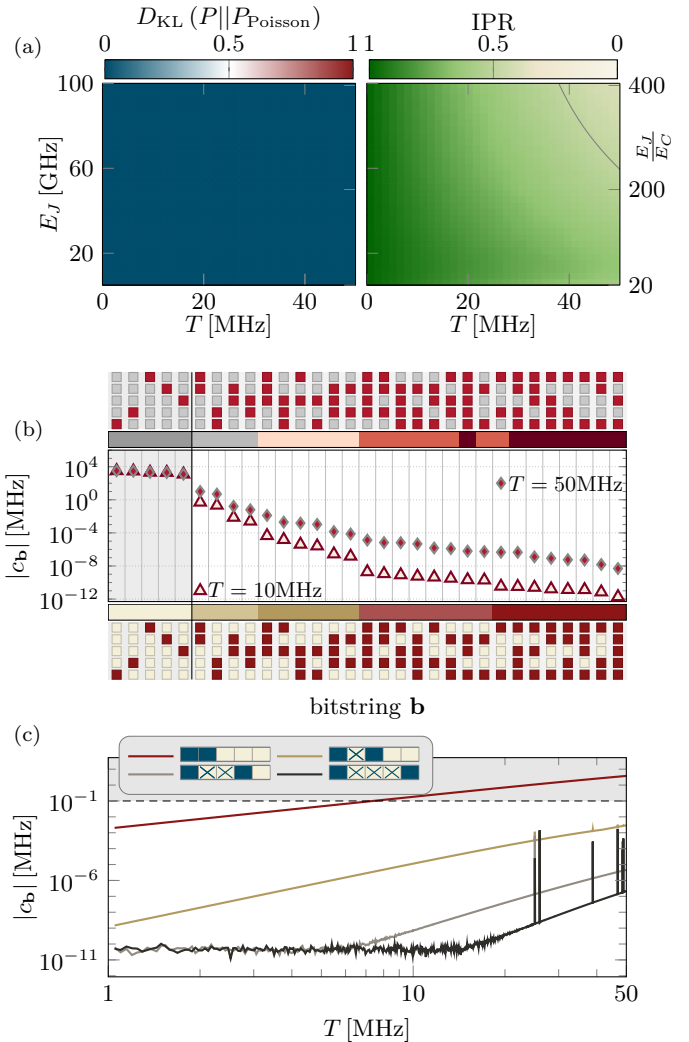


FIG. 7. **Summary of diagnostics for Delft/Google parameters.** (a) Phase diagram in terms of spectral statistics (left) and IPR (right), akin to Fig. 3. (b) and (c) Walsh analysis, akin to Fig. 6.

is also available, but in its operation another strategy is used: extra hardware is introduced to make T tunable. Being able to set the effective T to zero (although only in a perturbative sense) of course eliminates the problem of delocalization, and in this latest Google work δE_J has been returned to a small value. Google made some major changes in its ‘Hamiltonian strategy’ in preceding years [9] that have led them to the current success.

Considering parameters appropriate for the recent Delft chips, we study again all our diagnostics, see Fig. 7. The phase diagrams of Fig. 7(a) show that the MBL-chaos transition has retreated to much larger T , with the KL calculation showing basically no departure from Poisson behavior, and the IPR showing only a small drop from one, showing that the dressing effect is much smaller than in the IBM case. But our Walsh diagnostic for a disorder realization with $\delta E_J = 7.5$ GHz, summarized in Fig. 7(b) and (c), shows that troubles have

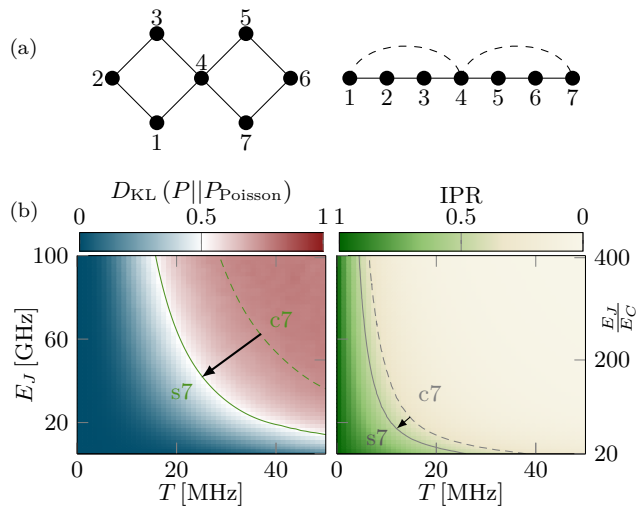


FIG. 8. **Surface 7 transmon geometry.** Phase diagram of seven coupled transmons, coupled in a surface 7 (s7) geometry (indicated on top of the figure). The inclusion of two additional couplings in comparison to a chain of seven transmons (c7) leads to significant shifts in the phase diagram calculated for IBM parameters, as illustrated in the left panel for the level statistics and in the right panel for the IPR. Shown on the left is the shift of the line indicating where the normalized KL divergence with regard to Poisson statistics has increased to 0.5 (see also Figs. 2 and 3). On the right we indicate the shift of the line indicating where the IPR drops below 0.5, akin to the lower panel in Fig. 3.

not entirely disappeared. Although definitely at a lower level, the higher-order terms of the τ -Hamiltonian are still present, with the ZZ danger threshold (dashed line) still reached. But this occurs only at around $T = 9$ MHz, about three times larger than for the IBM parameters. So, dangerous MBL phenomenology is still lurking in the wings, even in this much more favorable setting.

C. Transmon arrays in higher dimensions

All the conclusions of the last few sections have been reached by calculations for transmons coupled in a one-dimensional chain geometry. However, actual quantum information architectures are two dimensional, and we have therefore also simulated the surface-7 layout [8, 29] as a minimal example in this category. The surface-7 chip comprises a pair of square plaquettes, which is obtained from a chain of seven transmons by including two additional couplings, see top panel of Fig. 8. (Google’s 53-qubit layout extends this principle to a large square array extension.)

The study of two dimensional geometries, or of one dimensional arrays shunted by long range connectors, is motivated by the realization that the case of strictly one dimensional chains is exceptional: in one dimension, ‘rare fluctuations’ with anomalously strong local disorder amplitudes may block the correlation between different parts of the system, en-

hancing the tendency to form a many-body localized state. In higher dimensions, such roadblocks become circumventable, which makes disorder far less efficient in inhibiting quantum transport. For an in-depth discussion of the effects of dimensionality on MBL we refer to Ref. [30].

Our simulation of the surface-7 architecture, where we have chosen IBM parameters for concreteness, is summarized in Fig. 8. The spectral and wave function statistics data indicates that, not surprisingly, chaotic traces are rather more prominent than in the one-dimensional simulations (and despite the fact that we nominally added only two extra couplings in comparison to a purely one-dimensional geometry). The bottom line of this study is that the comfort zone introduced by the large-disorder schemes is considerably diminished when including higher-dimensional couplings.

V. CONCLUSIONS

The subject of this study was an application of state-of-the-art methodology of many-body localization theory to realistic models of present-day transmon computing platforms. In the mindset of the localization theorist, all transmon quantum information hardware has in common that it operates in a regime where the tendency of quantum states to spread by inter-qubit coupling is blocked by the detuning of qubit frequencies — the many body localized phase. Within this phase, there is considerable freedom for the realization of localization protected architectures, different strategies including weak coupling at weak detuning (IBM), or strong intentionally introduced detuning interspersed by sporadic and incomplete coupling (Delft/Google). On this background, we explored the integrity of different localized phases, in view of the omnipresent phase boundary to a chaotic sea of uncontrollable state fluctuations in the limit of too weak detuning and/or too strong coupling.

The single most important insight of this study is just how extended the twilight zone of partially compromised quantum states already is before reaching the boundary to hard quantum chaos. One may object that the existence of a crossover zone is owed to the smallness of the transmon arrays of 5-10 units studied in this work. However, it has to be kept in mind that the dimension of the random Hilbert spaces in which the many body quantum states live is exponential in these numbers and large by any (numerical) standard of localization theory. This indicates that ‘finite-size effects’ in these systems are notorious and must be kept in mind for computing architectures of technologically relevant scales.

A second unexpected finding is that early indicators of chaotic fluctuations show in different ways in different observables. Among these, the least responsive observable is many body spectral statistics, the most frequently applied diagnostics of the MBL/chaos transition. Unfortunately, the computational states themselves respond far more sensitively to departures from the limit of extreme localization. We have observed this tendency in the standard observable for wave function statistics, the inverse participation ratios, where Fig. 3 shows tendencies to strong wave function spreading already in pa-

parameter regimes where spectral statistics suggests complete safety. Surprisingly, however, the Walsh transform diagnostic — which is uncommon in MBL theory, but highly relevant as an applied quality indicator for the integrity of physical qubit states — responds even more sensitively to parameter changes away from the deep localization limit. Expressed in the language of quantum information technology, it indicates strong ZZ coupling and the onset of ZZZ coupling already in regimes where the participation ratios are asymptomatic.

What is the applied significance of these observations? All transmon based quantum technology operates in a tension field defined by the desire to optimally protect (detune) and efficiently operate (couple). However, there are different master strategies to resolve this conflict of interests, the IBM ‘weak coupling/weak detuning’ approach and the Delft/Google ‘transient-incomplete coupling/strong detuning’ strategy being diametrically opposed solutions. Our study indicates that the IBM strategy is significantly more vulnerable to chaotic fluctuations. We go as far as to speculate that it may not sustain the generalization to larger and two-dimensionally

interconnected array geometries required by more complex applications. However, regardless of what hardware is realized, the findings of this work indicate that the shadows of the chaotic phase are much longer than one might have hoped and that careful scrutiny of chaotic influences must be an integral part of future transmon device engineering.

ACKNOWLEDGMENTS

We thank S. Börner for collaboration on an initial project [31] studying incipient chaos in classical transmon systems. We acknowledge partial support from the Deutsche Forschungsgemeinschaft (DFG) under Germany’s Excellence Strategy Cluster of Excellence Matter and Light for Quantum Computing (ML4Q) EXC 2004/1 390534769 and within the CRC network TR 183 (project grant 277101999) as part of projects A04 and C05. The numerical simulations were performed on the CHEOPS cluster at RRZK Cologne and the JUWELS cluster at the Forschungszentrum Jülich.

-
- [1] In the MBL literature these are called p -bits and l -bits; we modify the notation to connect to modern quantum-information usage.
- [2] D. A. Huse, R. Nandkishore, and V. Oganesyan, Phenomenology of fully many-body-localized systems, *Phys. Rev. B* **90**, 174202 (2014).
- [3] M. Serbyn, Z. Papić, and D. A. Abanin, Local Conservation Laws and the Structure of the Many-Body Localized States, *Phys. Rev. Lett.* **111**, 127201 (2013).
- [4] J. Ku, X. Xu, M. Brink, D. C. McKay, J. B. Hertzberg, M. H. Ansari, and B. L. T. Plourde, Suppression of Unwanted ZZ Interactions in a Hybrid Two-Qubit System, *Phys. Rev. Lett.* **125**, 200504 (2020).
- [5] T. Orell, A. A. Michailidis, M. Serbyn, and M. Silveri, Probing the many-body localization phase transition with superconducting circuits, *Phys. Rev. B* **100**, 134504 (2019).
- [6] R. E. Throckmorton and S. Das Sarma, Studying many-body localization in exchange-coupled electron spin qubits using spin-spin correlations, arXiv e-prints (2020), 2009.04457.
- [7] We may incidentally remark that this work started from a project study [31] on *classical* chaos in the transmon system. Classically, the transmon Hamiltonian Eq. (1) describes a system of coupled mathematical pendula of mass $m = 1/8E_C$ and gravitational acceleration $g = 8E_C E_J$ (in units where $\hbar = 1$ and $\ell = 1$ (pendulum length)). Nonlinearly coupled pendula generally show a transition from integrable motion at low energies to hard chaos at high energies. (There are desktop gimmicks with just two coupled masses demonstrating the phenomenon.) The surprising observation of the project was that already the classical two transmon Hamiltonian, at excitation energies matching those of QC applications with 0 and 1 qubit states, was turning unstable. The generalization to ten coupled oscillators made the situation worse, with Lyapunov exponents signaling uncontrollable dynamics at time scales way below the scales set by typical coherence times. Manifestations of quantum chaos tend to be a bit more mellow than those of hard classical chaos, and the quantum transmon array is no exception to this rule. Nevertheless our above analysis shows that the situation is not nearly as well controlled as one might wish for.
- [8] R. Versluis, S. Poletto, N. Khammassi, B. Tarasinski, N. Haider, D. J. Michalak, A. Bruno, K. Bertels, and L. DiCarlo, Scalable Quantum Circuit and Control for a Superconducting Surface Code, *Phys. Rev. Applied* **8**, 034021 (2017).
- [9] F. Arute, K. Arya, R. Babbush, D. Bacon, J. C. Bardin, R. Barends, R. Biswas, S. Boixo, F. G. S. L. Brandao, D. A. Buell, B. Burkett, Y. Chen, Z. Chen, B. Chiaro, R. Collins, W. Courtney, A. Dunsworth, E. Farhi, B. Foxen, A. Fowler, C. Gidney, M. Giustina, R. Graff, K. Guerin, S. Habegger, M. P. Harrigan, M. J. Hartmann, A. Ho, M. Hoffmann, T. Huang, T. S. Humble, S. V. Isakov, E. Jeffrey, Z. Jiang, D. Kafri, K. Kechedzhi, J. Kelly, P. V. Klimov, S. Knysh, A. Korotkov, F. Kostritsa, D. Landhuis, M. Lindmark, E. Lucero, D. Lyakh, S. Mandrà, J. R. McClean, M. McEwen, A. Megrant, X. Mi, K. Michielsen, M. Mohseni, J. Mutus, O. Naaman, M. Neeley, C. Neill, M. Y. Niu, E. Ostby, A. Petukhov, J. C. Platt, C. Quintana, E. G. Rieffel, P. Roushan, N. C. Rubin, D. Sank, K. J. Satzinger, V. Smelyanskiy, K. J. Sung, M. D. Trevithick, A. Vainsencher, B. Villalonga, T. White, Z. J. Yao, P. Yeh, A. Zalcman, H. Neven, and J. M. Martinis, Quantum supremacy using a programmable superconducting processor, *Nature* **574**, 505 (2019).
- [10] A. D. Córcoles, A. Kandala, A. Javadi-Abhari, D. T. McClure, A. W. Cross, K. Temme, P. D. Nation, M. Steffen, and J. M. Gambetta, Challenges and Opportunities of Near-Term Quantum Computing Systems, *Proceedings of the IEEE* **108**, 1338 (2020).
- [11] J. Koch, T. M. Yu, J. Gambetta, A. A. Houck, D. I. Schuster, J. Majer, A. Blais, M. H. Devoret, S. M. Girvin, and R. J. Schoelkopf, Charge-insensitive qubit design derived from the Cooper pair box, *Phys. Rev. A* **76**, 042319 (2007).
- [12] A. Blais, A. L. Grimsmo, S. M. Girvin, and A. Wallraff, Circuit Quantum Electrodynamics, (2020), arXiv:2005.12667.
- [13] N. Macé, F. Alet, and N. Laflorencie, Multifractal Scalings Across the Many-Body Localization Transition, *Phys. Rev. Lett.* **123**, 180601 (2019).

- [14] For the $N = 10$ transmon chain at hand, this manifold contains a total of 2002 different states.
- [15] V. Oganessian and D. A. Huse, Localization of interacting fermions at high temperature, *Phys. Rev. B* **75**, 155111 (2007).
- [16] F. Monteiro, T. Micklitz, M. Tezuka, and A. Altland, Fock Space Localization in the Sachdev-Ye-Kitaev Model, (2020), arXiv:2005.12809.
- [17] M. Mézard and A. Montanari, *Information, Physics, and Computation* (Oxford University Press, 2009).
- [18] F. Evers and A. D. Mirlin, Anderson transitions, *Rev. Mod. Phys.* **80**, 1355 (2008).
- [19] Y. A. Farkov, P. Manchanda, and A. H. Siddiqi, Introduction to Walsh Analysis and Wavelets, in, *Construction of Wavelets Through Walsh Functions. Industrial and Applied Mathematics*. Springer, Singapore , 1 (2019).
- [20] K. Michielsen, M. Nocon, D. Willsch, F. Jin, T. Lippert, and H. De Raedt, Benchmarking gate-based quantum computers, *Computer Physics Communications* **220**, 44 (2017).
- [21] N. Moll, P. Barkoutsos, L. S. Bishop, J. M. Chow, A. Cross, D. J. Egger, S. Filipp, A. Fuhrer, J. M. Gambetta, M. Ganzhorn, A. Kandala, A. Mezzacapo, P. Müller, W. Riess, G. Salis, J. Smolin, I. Tavernelli, and K. Temme, Quantum optimization using variational algorithms on near-term quantum devices, *Quantum Science and Technology* **3**, 030503 (2018).
- [22] S. Sheldon, E. Magesan, J. M. Chow, and J. M. Gambetta, Procedure for systematically tuning up cross-talk in the cross-resonance gate, *Phys. Rev. A* **93**, 060302 (2016).
- [23] M. Khezri, J. Dressel, and A. N. Korotkov, Qubit measurement error from coupling with a detuned neighbor in circuit QED, *Phys. Rev. A* **92**, 052306 (2015).
- [24] A. Galiatdinov, A. N. Korotkov, and J. M. Martinis, Resonator–zero-qubit architecture for superconducting qubits, *Phys. Rev. A* **85**, 042321 (2012).
- [25] J. C. Pommerening and D. P. DiVincenzo, What is measured when a qubit measurement is performed on a multiqubit chip, *Phys. Rev. A* **102**, 032623 (2020).
- [26] E. Magesan and J. M. Gambetta, Effective Hamiltonian models of the cross-resonance gate, *Phys. Rev. A* **101**, 052308 (2020).
- [27] N. Sundaresan, I. Lauer, E. Pritchett, E. Magesan, P. Jurcevic, and J. M. Gambetta, Reducing unitary and spectator errors in cross resonance with optimized rotary echoes (2020), arXiv:2007.02925 [quant-ph].
- [28] D. W. Leung, I. L. Chuang, F. Yamaguchi, and Y. Yamamoto, Efficient implementation of coupled logic gates for quantum computation, *Phys. Rev. A* **61**, 042310 (2000).
- [29] C. K. Andersen, A. Remm, S. Lazar, S. Krinner, N. Lacroix, G. J. Norris, M. Gabureac, C. Eichler, and A. Wallraff, Repeated quantum error detection in a surface code, *Nature Physics* **16**, 875 (2020).
- [30] A. C. Potter, R. Vasseur, and S. A. Parameswaran, Universal Properties of Many-Body Delocalization Transitions, *Phys. Rev. X* **5**, 031033 (2015).
- [31] S.-D. Börner, *Classical Chaos in Transmon Qubit Arrays*, Bachelor Thesis, University of Cologne (2020).